Journal of Industrial and Engineering Chemistry 109 (2022) 510–520

Contents lists available at ScienceDirect

Journal of Industrial and Engineering Chemistry

journal homepage: www.elsevier.com/locate/jiec

Enhanced crystallization and properties of poly(ethylene terephthalate) nanocomposites with zeolites from 3D to 2D topologies

Wei Zhang [a], Hongbin Zhang [b], Liping Yang [c], Yi Tang [d], Ping Tang [a,*]

[a] State Key Laboratory of Molecular Engineering of Polymers, Department of Macromolecular Science, Fudan University, Shanghai 200433, China
[b] Institute for Preservation of Chinese Ancient Books, Fudan University Library, Fudan University, 200433 Shanghai, China
[c] Wankai New Material Co., Ltd., Haining 314415, China
[d] Department of Chemistry, Laboratory of Advanced Materials, Collaborative Innovation Center of Chemistry for Energy Materials and Shanghai Key Laboratory of Molecular Catalysis and Innovative Materials, Fudan University, Shanghai 200433, China

ARTICLE INFO

Article history:
Received 31 December 2021
Revised 14 February 2022
Accepted 18 February 2022
Available online 24 February 2022

Keywords:
polymer crystallization
zeolites
nucleation agent
dispersion
exfoliation
poly(ethylene terephthalate)

ABSTRACT

To improve the low crystallization rate and long molding cycle of Poly(ethylene terephthalate) (PET), series of PET nanocomposites incorporated small quantities of zeolites with different topologies were blended by melt compounding. The nucleation influence of 3-dimensional zeolites Y, ZSM-5 and 2-dimensional zeolite MCM-22P on the crystallization manner of PET was analyzed by non-isothermal and isothermal crystallization, quantitative evaluation of nanoparticle dispersion and morphology of nanoparticles. The results show that all PET/zeolite nanocomposites exhibit higher crystallization temperature and faster crystallization rate than PET due to large specific surface area of zeolites and their superior dispersion in the PET matrix. Among them, PET/MCM-22P nanocomposites remarkably improved the crystallization behavior, thermal stability and oxygen barrier properties, which is related to the layered morphology of MCM-22P and hydrogen bond interactions between MCM-22P and PET. It is revealed that MCM-22P can provide more heterogeneous nucleation sites for PET by exfoliation in melting compounding. Furthermore, the nucleation mechanism induced by MCM-22P was investigated by the means of Mozhishen method, Avrami equation and theory of Hoffman-Lauritzen. The results indicate that the incorporation of MCM-22P can decrease the free energy of nucleation and fold surface in PET crystallization process, thus improving the crystallinity.

Introduction

Poly(ethylene terephthalate) (PET) is one of the most important semi-crystalline thermoplastic materials with extensive applications in packaging films and bottles, fibers as well as engineering plastics due to its outstanding mechanical properties and cost efficiency [1,2]. The ultimate performance of PET strongly depends on its condensed structure, which is mainly determined by its crystallization behavior. Introducing a small number of nucleating agents with high compatibility to polymers can reduce the barrier of nucleation energy in crystallization process by providing more heterogeneous nucleation sites [3]. To advance the crystallization performance, a large number of organic fillers have been used as nucleating agents, such as carboxylate alkali metal salt [4,5] and ionomers like Surlyn [6], Acyln [7] and SMA ionomers [8]. However, some recent works show that organic salts always suffer from thermal degradation in melting compounding with PET, resulting in inferior properties of composites [4,7,9,10].

Inorganic nanoparticles such as clays [11], carbon nanotubes [12], and graphenes [13] possess potential applications to advance the behavior of PET crystallization. Among them, silicates have been applied as nucleating agents for polymer due to their high specific surface area and excellent thermal stability [14,15]. Zeolite molecular sieve is one of the most important silicates with high specific surface area, uniform pore topology and large pore volume [16–18]. Recently, polymer nanocomposites with zeolites as additives have attracted great interest in enhancing the thermal and permeability properties in industry, such as LDPE/zeolite, PP/zeolite, and PU/zeolite nanocomposites [15,16,19–21]. The preparation of nanocomposites with individual nanoparticles as nucleating agents is a challenging issue due to the high surface energy and Van der Walls interaction between nanofillers [22]. Therefore, uniform dispersion of the added nanoparticles as effec-

* Corresponding author.
E-mail address: pingtang@fudan.edu.cn (P. Tang).

https://doi.org/10.1016/j.jiec.2022.02.038
1226-086X/

tive nucleating agents is the key to improve the crystallinity of PET [23–26]. However, the effect of silicate zeolites with different topologies on the crystallization of PET has not been investigated yet. At the same time, the quantification of dispersion for inclusions in polymer nanocomposites is crucial to improve the performance which hasn't been analyzed in detail either.

In this paper, the PET/zeolite nanocomposites by incorporated 3D zeolite Y, ZSM-5 and 2D zeolite MCM-22P were prepared by melt compounding to investigate the crystallization process. It is demonstrated that all zeolites obviously improve the crystallization behavior of PET as nucleation agents and have superior dispersion in the PET matrix by quantitative evaluation, especially the MCM-22P. The splendid effects of MCM-22P were found that MCM-22P had a favorable compatibility with PET due to layered morphology and surface hydroxy groups. Besides, 2D MCM-22P can be exfoliated further during the melting compounding process, providing abundant nucleation sites for PET. The processes of non-isothermal and isothermal crystallization in PET/MCM-22P nanocomposites with a certain ratio (0.1%, 0.5%, 1% and 2%) was explored by the means of Mozhishen method, Avrami equation and Hoffman–Lauritzen theory.

Materials and experiments

Materials

PET (trade name WK811) with an intrinsic viscosity of 0.79 dL/g was provided by Wankai New Material Co., Ltd., China. Zeolites Na-Y (NKF-7SC) and ZSM-5 (NKF-7) were purchased from the Catalyst Plant of Nankai University. Silica sol (40 wt%, Ludox), $NaAlO_2$ (54.49% Al_2O_3, 41.07% Na_2O, 4.44% H_2O, Sigma-Aldrich), NaOH (AR grade) from Shanghai Chemical Co. China, and hexamethyleneimine (HMI, TCL, 99.9%) were used to synthesize 2D zeolite MCM-22P. Other chemicals were obtained from the Sinopharm Chemical Reagent. And all of them are analytical grade and used without further purification.

Synthesis of Na-ZSM-5 and MCM-22P

Na-ZSM-5 zeolite was prepared by exchanging zeolite ZSM-5 with the aqueous solutions of sodium nitrate (analytical grade) from Sinopharm under the concentration of 2.0 mol/L for 3 h at 90 °C in an oil bath, and repeated two more times. After exchange treatment, the solid products were separated by filtration and washed with deionized water for three times, and then they were dried at 353 K overnight. Na-ZSM-5 and Na-Y were used in this work.

2D MCM-22P zeolite was synthesized hydrothermally with silica sol, $NaAlO_2$, NaOH, hexamethyleneimine, and deionized water in accordance with the gel composition 1 SiO_2 : 0.020 Al_2O_3 : 0.15 NaOH : 0.2 HMI : 30 H_2O. At first, the gel was stirred for 1 hour, then transferred into a 100 mL Teflon-lined autoclave, and then heated at 423 K with 45 rpm for 4 days. The obtained solid product was separated by centrifugation, then washed with deionized water to pH < 9, and dried at 353 K for 12 hours.

Preparation of PET/zeolite nanocomposites

The PET nanocomposites were prepared by melting compounding with three different topology zeolites as scheme 1. PET was dried in the vacuum oven at 110 ℃ for 24 h to prevent hydrolysis in the process of the melt compounding. PET was blended with zeolites at 280 ℃ in a torque rheometer (Changkai CTR-300, China) at a rotor speed of 60 rpm for 5 minutes.

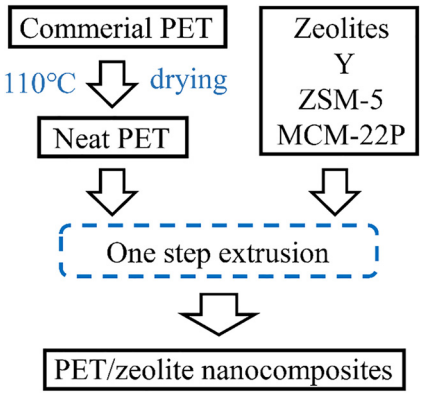

Scheme 1. Flowchart of the production of PET/zeolite nanocomposites with different topologies of zeolites.

Characterization

The crystalline structures of zeolites were characterized by X-ray diffraction (XRD) (D8 Advance, Bruker), operating with Cu Kα radiation (λ = 1.54 Å), 40 kV, 40 mA. The N_2-adsorption isotherms were measured by a Micromeritics ASAP-2010 instrument and the specific surface area were determined by an Autosorb IQ_2 analyzer using BET methods at liquid-nitrogen temperature. The morphology of PET/zeolite nanocomposites was examined by Ultra 55 field scanning electron microscopy (Zeiss, Germany) equipped with an energy dispersion X-ray spectrometer (EDS), and their chemical compositions were determined by EDS.

The crystallization and melting behaviors of PET and PET/zeolite nanocomposites were analyzed by isothermal and non-isothermal process with DSC Q2000 (TA instruments) in the nitrogen atmosphere, the concrete steps are in Supporting Information [9]. The thermal stability behavior was characterized by using thermogravimetric analyzer Pyris1, PE instrument. A Labthink Basic 202 was used to measure the oxygen permeation at 23 °C.

Fluorescent micrographs were obtained with the confocal laser scanning microscope (CLSM) (Nikon C2+, Japan) to observe the dispersion of zeolites in PET matrix and for further quantification evaluation. The morphology of zeolite in PET matrix was investigated by TEM HT7800 (Hitachi, Japan) and FETEM Tecnai G2 (FEI, the USA) with ultra-thin section prepared by cryogenic-sectioning in a Leica system (UCT/EMFCS). The solid state ^{14}Si NMR and ^{27}Al NMR spectra were recorded on Bruker Avance III at 25 ℃ at 400 MHz. ATR FTIR spectra were recorded on Thermo-Fisher Nicolet 6700 at wavenumber between 400 cm^{-1} and 4000 cm^{-1} with 64 scans.

Results and discussion

Characterization of zeolites with different frameworks

Microporous zeolites of distinct framework types (zeolite Y, ZSM-5 and MCM-22P) from 3D to 2D analogues have been employed here as the typical additives or nucleation agents to assess their effect on the crystallization of PET. Zeolite Y and ZSM-5 are important commercial zeolites for catalytic application [27–29]. Y zeolite (FAU framework) has identical faujasite-cage structures with three-dimensional 12-MR channels (Fig. 1 a1, [111] 7.4x7.4 Å), while ZSM-5 zeolite (MFI framework) consists of the intersected sinusoidal and linear 10-MR channels along a or b axis (Fig. 1 b1, [100] 5.1x5.5 Å, [010] 5.3x5.6 Å). The first layered zeolite and the most studied 2D zeolites so far are the MWW

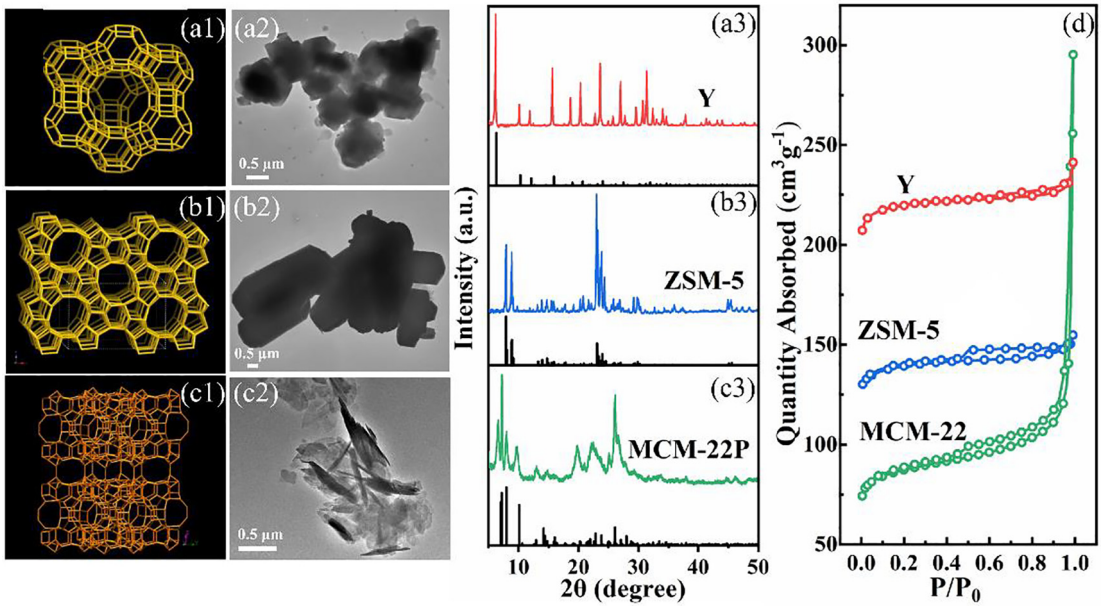

Fig. 1. Topology structure (a1, b1, c1), TEM images (a2, b2, c2), X-ray patterns (a3, b3, c3) for zeolites of (a) Y, (b) ZSM-5 and (c) MCM-22P and (d) N_2 adsorption–desorption isotherms of zeolites (the vertical axis value of ZSM-5 increased by 50 for clarity).

zeolites [30–32]. MCM-22P is the layered precursor of MCM-22 zeolite which comprises layered nanosheets of MWW topology with a uniform thickness of 2.5 nm stacked in register (Fig. 1 c1, [001] 4.0x5.5 Å, [001] 4.1x5.1 Å). The TEM images of zeolite Y, ZSM-5 and MCM-22P are shown in a2, b2 and c2 in Fig. 1, respectively. It is obvious that Y (octahedral-shape) and ZSM-5 (coffin-shape) are of 3D framework while MCM-22P is of 2D layer framework, according to their different crystal structures and growth directions. Besides, the Material studio images and data of Y, ZSM-5 and MCM-22P are shown in Fig. S1 and Table SI in Supporting Information. The yellow part represents the Al/Si atom and the red part refers to the O atom associated with frameworks shown a1, b1 and c1 in Fig. 1.

The XRD patterns of three typical zeolite samples (zeolite Y, ZSM-5 and MCM-22P) between 5° and 50° are presented a3, b3, c3 in Fig. 1, which shows the related feature peaks in accordance with that of FAU, MFI and MWW type structure (see the black lines for the characteristic peaks at the bottom), respectively. All the samples exhibit not any other impure phases. Besides, the textural properties and porosities are characterized by N_2 sorption. The adsorption–desorption isotherms of Y, ZSM-5 and MCM-22P zeolites after calcination are shown in Fig. 1 d. For 3D zeolites, Y and ZSM-5 behave the similar N_2 sorption isotherms with almost no hysteresis loop and only a steep slope at a relative low pressure ($P/P_0 < 0.2$), illustrating their well-maintained microporous structures without mesopore volume as shown in pore size distribution curves in Fig. S2 of Supporting Information. For the 2D analogues, MCM-22 presents a hysteresis loop that starts at $P/P_0 = 0.45$ and has greatly increased at partial pressure $P/P_0 > 0.9$, indicating the layered stacking structure [33]. The detailed textural properties of three zeolite samples are summarized in Table 1. Compared with 3D conventional Y and ZSM-5 zeolite, the external surface area and mesopore volume of MCM-22 sample are remarkably higher, further confirming the characteristics of 2D layered zeolites as shown in Fig. S2.

SEM was used to detect the morphology of PET/nanocomposites as shown a1, b1, c1, d1 of Fig. S3 in Supporting Information. Besides, EDS characterization was employed to investigate the elemental composition of nanocomposites and dispersion of zeolites in PET matrix. As shown in Fig. S3, the zeolite contained the elements of Al (b4, c4, d4), Si (b5, c5, d5) and O (a3, b3, c3, d3), while neat PET contained elements C (a2, b2, c2, d2) and O. From the perspective of the element distribution, Al/Si element had good dispersity in the PET/zeolite nanocomposites, indicating that nanoparticles were composited with PET matrix completely.

Non-isothermal crystallization behavior and properties of PET/zeolite nanocomposites

The crystallization and melting process of PET and PET/zeolite nanocomposites are explored under non-isothermal processes in order to distinguish the effect of three zeolites with different topologies and especially MCM-22P with different contents on the crystallization behavior of PET [9]. The DSC curves of neat PET and PET/zeolite nanocomposites at the heating/cooling rate of 10 ℃/min were illustrated in Fig. 2 a1-a2, and the results of parameters were summarized in Table 2. The most intuitive parameters to estimate crystallization process are the cold-crystallization temperature T_{cc} in the heating curve and the melt-crystallization temperature T_{mc} in the cooling curve. The value of

Table 1
Textural data of the zeolite samples after calcination in nitrogen at 550 ℃ for 5 h.

Sample	S^a_{BET}	S^b_{micro}	S^b_{exte}	V^c_{micro}	V^c_{meso}	V^c_{total}
MCM-22	339.6	285.8	53.8	0.112	0.356	0.468
Y	907.4	883.1	24.3	0.329	0.060	0.389
ZSM-5	353.9	328.3	25.6	0.127	0.049	0.176

[a]Specific surface area determined by BET methods, [b] the micropore and external surface area, [c] the micropore, mesopore and total volume.

Table 2
Non-isothermal melt and crystallization parameters results of PET/zeolite and PET/M22P nanocomposites.

Samples	T_g℃	T_{cc}℃	T_m℃	ΔH_mJ/g	T_{onset}℃	T_{mc}℃	ΔH_{mc}J/g	ΔT_{mc}℃	X_c%
PET	72.5	134.3	254.5	35.7	205.4	176.6	34.6	77.9	29.4
PET/1%Y	74.8	132.0	253.4	38.2	223.9	215.2	45.9	38.2	39.0
PET/1%ZSM-5	76.5	131.9	253.5	36.9	224.0	215.1	44.6	38.4	37.9
PET/1%MCM-22P	74.3	121.0	253.9	40.3	225.2	216.5	47.6	37.4	40.5
PET/M22P0.1	75.5	127.1	255.1	39.1	216.3	208.9	39.6	46.2	33.7
PET/M22P0.5	74.4	124.4	254.0	38.4	217.7	209.9	40.9	44.1	34.8
PET/M22P2.0	74.5	127.0	255.6	40.1	222.2	213.6	46.6	42.0	39.6

T_{cc} shifted to lower temperature after the incorporation of zeolites compared to neat PET as shown in Fig. 2 a1, and the values of onset crystallization temperature T_{onset} and T_{mc} tend to a higher temperature at the same time, corresponding to excellent crystallization performance. Lower T_{cc} and higher T_{mc} values of PET/zeolite nanocomposites indicate that both two crystallization processes are more inclined to proceed, which can be attributed to more interfaces provided by zeolites. On one hand, the nano-scale interfaces in the polymer matrix can act as heterogeneous nucleation sites for polymer chain to accelerate crystallization. On the other hand, the effective interfaces can promote the further growth of crystal nuclei and prevent the crystal nucleus from being melted again by the surrounding matrix [10]. Besides, the interface energy between zeolites and PET matrix is small due to the superior compatibility, thus the polymer chains are easily arranged in the interface region, and the formation of new interfaces will effectively increase the number of crystal nuclei in the system [34,35]. The T_{cc} and T_{mc} of nanocomposites with zeolite were decreased by 2–10 ℃ and increased by 37–40 ℃ compared to neat PET respectively, which confirmed that all three zeolites are efficient heterogeneous nucleating agents.

Generally, the supercooling temperature ΔT_{mc} ($\Delta T_{mc} = T_m - T_{mc}$), can quantitively characterize the process of crystallization and efficiency of nucleation. It is obvious that ΔT_{mc} was decreased by about 40 ℃ after the addition of zeolites, especially 2D MCM-22P, indicating faster crystallization rate and better nucleation efficiency for PET nanocomposites. Relative crystallinity X_C is expressed as the percentage ratio of crystallization enthalpy ΔH_{mc} to ΔH_f [36], verifying the degree of molecular order and crystallization efficiency. X_C of PET was increased from 29.4% to 39.0% of PET/Y, to 37.9% of PET/ZSM-5 and to 40.5% of PET/MCM-22P, reflecting that the addition of zeolites improved the crystallinity of neat PET. Among the three zeolites, MCM-22P behaves the most distinguished nucleation efficiency due to its specific 2D layered structure and superior dispersion in PET. The T_{cc} and T_{mc} of PET/MCM-22P were approximately 13 ℃ lower and 40 ℃ higher than those of neat PET, respectively. However, the other two 3D zeolites Y and ZSM-5 exhibit similar nucleation ability due to analogical structures, indicating that the influence of pore size in 3D topology is negligible.

Due to the remarkable performance of PET/MCM-22P, different contents of MCM-22P in PET/MCM-22P nanocomposites were further investigated by non-isothermal crystallization curves to explore the nucleation effect of MCM-22P on PET as shown in b1-b2 of Fig. 2 and Table 2. It is clear that the addition of only a small amount of 1.0 wt.% of MCM-22P can increase the T_{mc} by about 30 ℃, thus significantly accelerating the crystallization rate and increasing the relative crystallinity of neat PET. On one hand, the nanocomposites behave more splendid crystallization performance with the increase of MCM-22P content due to more nucleation sites when the added content is relatively small. On the other hand, when the content of MCM-22P exceeds 1.0 wt.%, the crystallization rate and relativity crystallinity of the nanocomposite as PET/M22P2.0 are inferior to PET/M22P1.0. It is illustrated that MCM-22P was more uniformly dispersed and provided more nucleating sites in PET/M22P1.0, thus resulting in higher crystallization temperature and faster crystallization rate compared to PET/M22P2.0.

In Fig. 2, c1 shows the TGA curves of PET and PET/zeolite nanocomposites. The decomposition onset of PET/zeolite nanocomposites was above 360 ℃, indicating that zeolites maintain solid-state without degradation at the processing temperature and can provide heterogeneous nucleating sites. The calculated data of TGA analysis are summarized in Table SII of Supporting Information. The temperatures at the 1.0 wt.%, 5.0 wt.% loss of weight, onset temperature of degradation of PET/zeolite nanocomposites are higher compared to PET. It can be attributed to the excellent thermal stability of zeolites and superior dispersion of zeolites in the PET matrix. Generally, the heat transfer of nanoparticles is faster than that of polymers and it is barely to cause heat concentration, thereby it can improve the thermal properties of PET. As shown in c2 of Fig. 2, the result oxygen permeation rate (OPR) of PET is 38.7 $cm^3\ m^{-2}\ day^{-1}\ atm^{-1}$ while the OPR results of PET/1%Y, PET/1%ZSM-5 and PET/1%MCM-22P were reduced to 24.8, 28.0, and 18.3 $cm^3\ m^{-2}\ day^{-1}\ atm^{-1}$, respectively. In particular, the promotion of oxygen barrier property is significant for the application of PET in industry which is attributed to hindered oxygen transfer and increased gas diffusion pathways by the increased relative crystallization degree and the formation of finer spherulite. It is proved that three zeolites are efficient nucleation agents and PET/zeolite nanocomposites exhibit considerably low oxygen permeation, which shows tremendous potential in packaging industry.

Quantitative evaluation of the zeolite dispersion in PET matrix

The properties of nanocomposites depend on the microstructures, especially in which the dispersion of nanoparticles plays an important role in improving the performance of nanocomposites. However, nanoparticles in polymer matrix can easily condense due to van der Waals attraction and electrostatic interactions [37]. In addition, the dispersion efficiency of nanoparticles depends on the compatibility with polymer matrix and its surface energy. To quantitively characterize the dispersion of three zeolites in PET matrix, fluorescent display agent Rhodamine B was introduced into zeolites to view the nanoparticles in PET with a CLSM microscope. The three zeolites in PET can be observed by fluorescent microscope after the addition of Rhodamine B and the characterization is based on the binarization of obtained micrographs by CLSM as Scheme 2. The area of each particle is calculated to distinguish the distribution and dispersion of zeolites by image analysis software. In this process, the bright-field images of nanoparticles in PET by CLSM are shown in Fig. 3 a1, b1, c1 and d1, and the fluorescence images in a2, b2, c2 and d2 are pictured to obtain the threshold value. Then the corresponding binary images are shown in a3, b3, c3 and d3 and the results of counted particle area distribution are in a4, b4, c4 and d4, in which N is the total particle number.

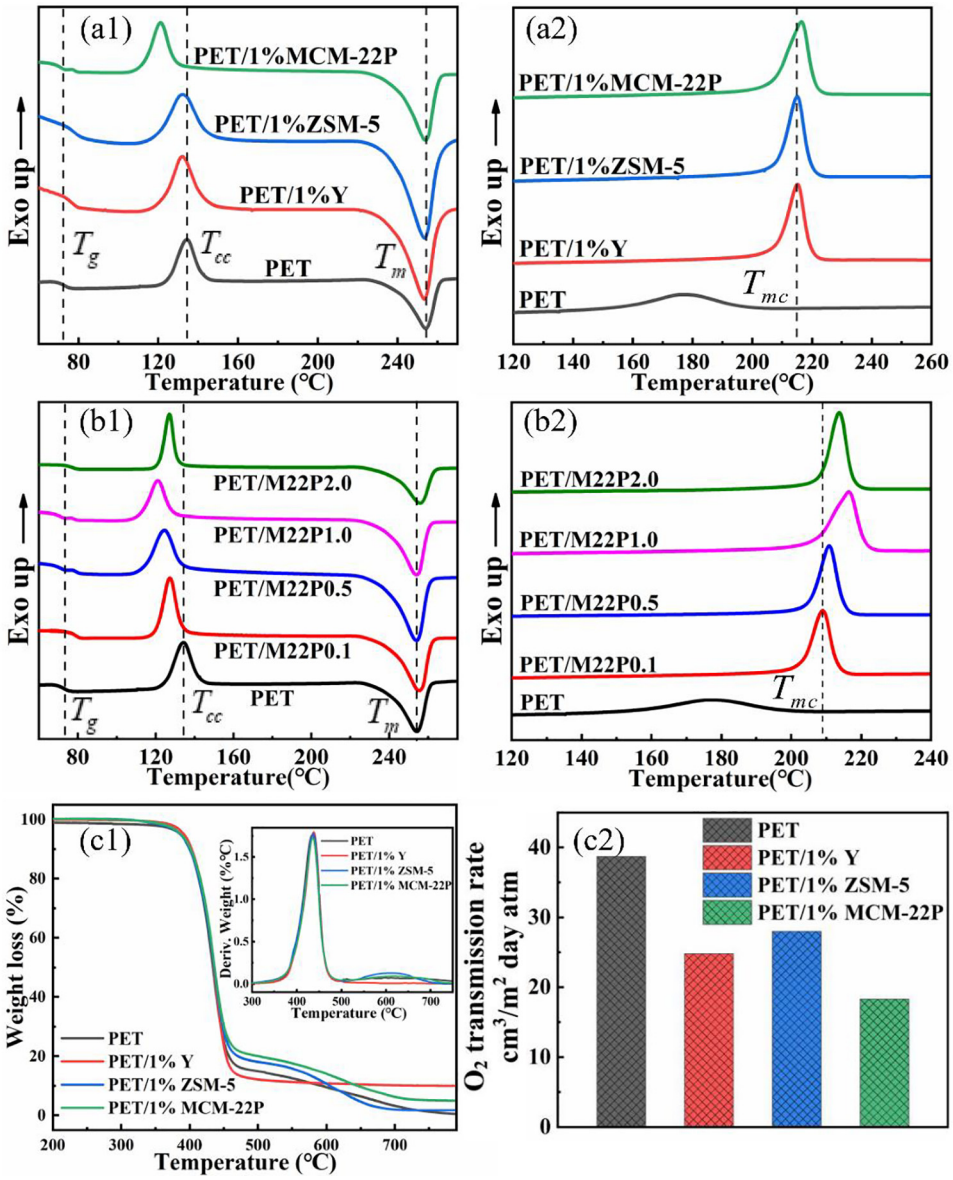

Fig. 2. Non-isothermal behaviors (a) PET/zeolite (a1: heating curve, a2: cooling curve) and (b) PET/M22P nanocomposites (b1: heating curve, b2: cooling curve) at rate of 10 ℃/min, (c1) TGA and their differential curves and (c2) OPR values of PET and PET/zeolite nanocomposites.

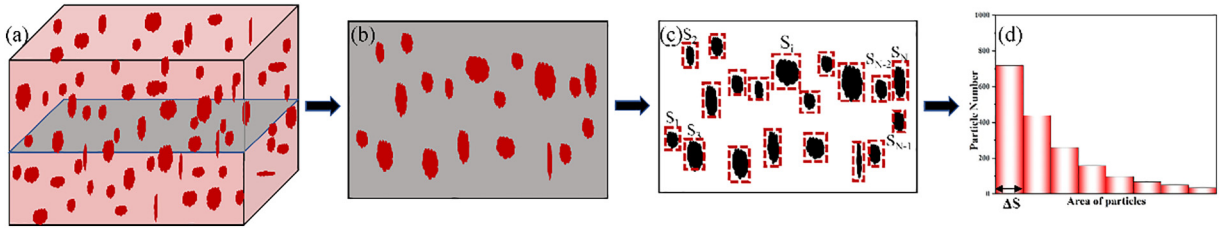

Scheme 2. Quantitative evaluation: (a) schematic morphologies of nanocomposites, (b) a cross-section from (a), (c) binarization of image (b), where the area of dispersed particles is measured and (d) the histogram based on the measurements of particle area (c).

To further quantify the dispersion of zeolite in PET matrix, the mean radius R_n of the nanoparticles is measured based on the binary images as Eq. (1), where N is the total number of particles, providing an intuitive method to analyze image features and particle dispersion degree. Besides, the number average S_n and the area average area S_s are defined as Eqs. (2) and (3) are obtained from the statistical results, and the dispersion index D is the ratio of S_s to S_n, reflecting the dispersion degree.

$$R_n = \frac{\sum_{i=1}^{N} \sqrt{\frac{S_i}{\pi}}}{N} \quad (1)$$

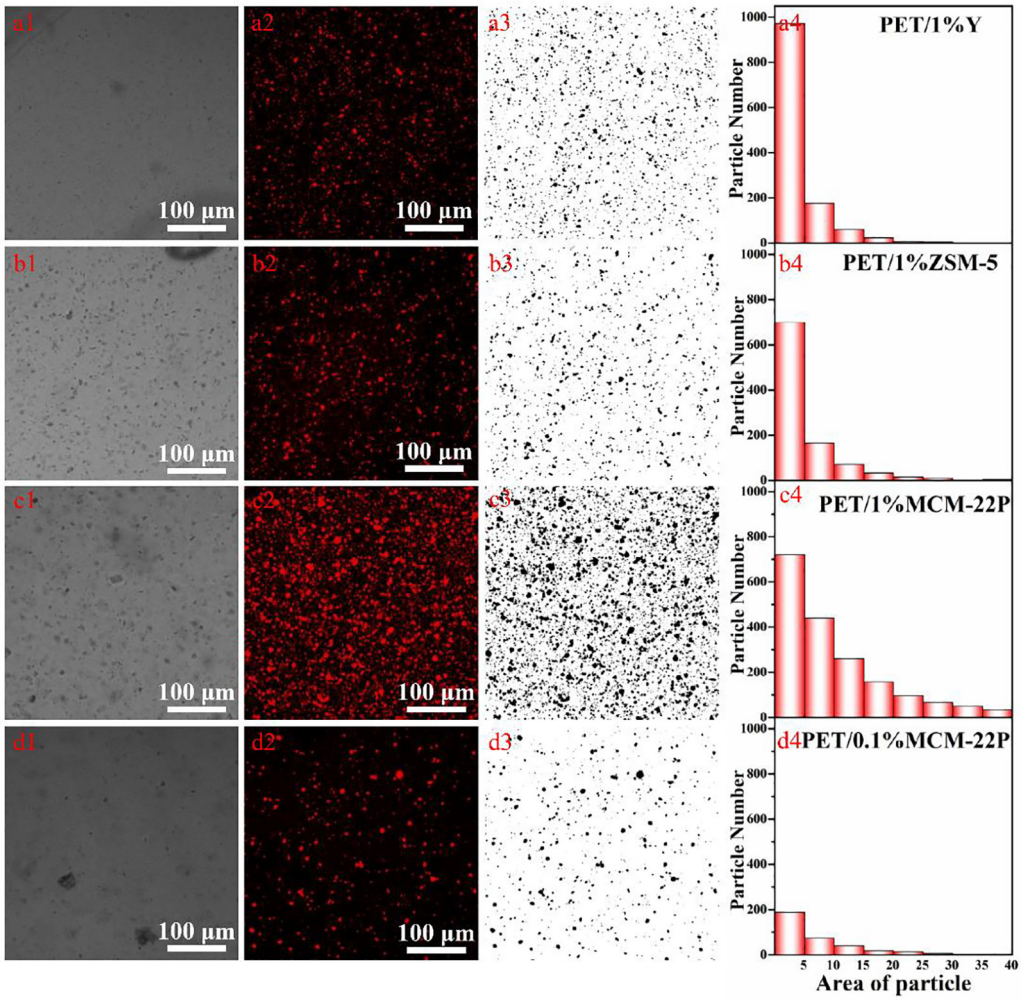

Fig. 3. The CLSM microscope images (first and second column) and corresponding binarization process (third column) and the nanoparticle area distribution (fourth column) of zeolites in PET: (a) PET/1%Y, (b) PET/1%ZSM-5, (c) PET/1%MCM-22P and (d) PET/0.1MCM-22P.

$$S_n = \frac{\sum_{i=1}^{N} S_i}{N} \tag{2}$$

$$S_s = \frac{\sum_{i=1}^{N} S_i \times S_i}{\sum_{i=1}^{N} S_i} \tag{3}$$

where S_i is the area of the particle i, $i = 1, 2, \ldots N$. Table 3 shows the essential parameters of nanocomposites filled with different types of zeolites. The dispersion results of two 3D zeolites Y and ZSM-5 are of little difference due to similar topologies, reflecting equivalent dispersion degree. However, the particle number N of 2D MCM-22P is much larger than the other two 3D zeolites due to the layered structure and exfoliation of MCM-22P which generated a larger number of platelets and provided much more nucleation sites in PET matrix. The internal volume of MCM-22P is larger compared to Y and ZSM-5, resulting in larger R_n, S_s and S_n. At the same time, the dispersion index D of MCM-22P equal to 1.9 is smaller than the other two zeolites, indicating a better dispersion degree of MCM-22P contributed by superior compatibility with PET. Furthermore, compared with PET/1%MCM-22P, the N of PET/0.1% MCM-22P is much smaller because of the little content of MCM-22P, providing fewer nucleation sites for PET. The S_s and S_n of the two PET/MCM-22P nanocomposites are essentially identical which results in similar dispersion index D, indicating the dispersion consistency of MCM-22P in PET. From the quantitative characterization of nanocomposites, it is confirmed that the three zeolites are all effective nucleation agents and behave good dispersion in PET matrix, showing a satisfactory agreement with non-isothermal crystallization in DSC curves. In particular, MCM-22P behaves the most distinguished dispersion efficiency due to its specific 2D layered topology, generating more heterogeneous nucleation sites by exfoliation and advancing the crystallization performance for PET.

Table 3
Quantitative evaluation parameters of zeolite dispersion in PET.

Sample	N	R_n	S_n	S_s	D
PET/1%ZSM-5	1001	1.13	5.02	11.1	2.22
PET/1%Y	1249	1.04	4.07	8.25	2.03
PET/1%MCM-22P	1516	1.46	7.97	15.2	1.90
PET/0.1%MCM-22P	342	1.38	7.21	13.5	1.87

Dispersal morphology of zeolites in PET matrix

To further investigate the dispersion of zeolite in PET and compatibility between zeolites and PET, especially the exfoliation of 2D MCM-22P, TEM pictures of nanocomposites are shown in a1, a2 and a3 of Fig. 4 and more pictures can be found in Supporting Information Fig. S4. The volume of 3D zeolite Y and ZSM-5 are slightly less than MCM-22P as observed in confocal microscope CLSM. MCM-22P platelets were uniformly dispersed in the PET matrix in a3 of Fig. 4, while the other two zeolites kept stackable structures in a1-a2 of Fig. 4 , indicating that MCM-22P has been exfoliated by the melt compounding with PET distinctly [32]. The zeolites can provide interfaces for PET to grow the nucleus, thus accelerating the crystallization process of PET. However, the exfoliated MCM-22P is better dispersed in PET matrix as discussed in the above quantitative evaluation of dispersion, and remarkably generates more nucleating sites, thus increasing the crystallization rate [38,39]. In comparison to MCM-22P, both 3D zeolite ZSM-5 and Y are more inclined to pile in PET matrix, resulting in fewer nucleating sites and a slower crystallization rate of PET nanocomposites. Morphologies of different content of MCM-22P in PET can be found in Fig. S5 of Supporting Information. The number of zeolite layers which was exfoliated obviously in PET/M22P1.0 is much more than that in PET/M22P0.1 and PET/M22P0.5, which can provide more nucleation sites for crystallization and contribute to better dispersion. However, the zeolite layers tend to aggregate together in PET matrix when the content of nucleating agent is up to 2%, resulting in inferior dispersion of PET/M22P2.0 compared to PET/M22P1.0.

To further investigate the degree of exfoliation of MCM-22P in PET matrix, the morphology of neat MCM-22P and different content of MCM-22P in PET are observed in a high-resolution FETEM microscope. MCM-22P presented a flake-like morphology with randomly stacked layers in a lamellar arrangement ~ 0.5 μm as shown in Fig. 4 b1, whereas MCM-22P has been exfoliated to platelets ~ 20 nm in PET/M22P1.0 (Fig. 4 b2) and ~ 70 nm in PET/M22P2.0 (Fig. 4 b3) after melt compounding. It is obvious that MCM-22P has been exfoliated to thinner platelets and the layer thickness of MCM-22P in PET/M22P1.0 are much thinner than that in PET/M22P2.0, since MCM-22P tends to pile up together with the increase of its content. The results are consistent with the non-isothermal crystallization data obtained from DSC curves in Fig. 2 b1-b2, both reflecting that the appropriate content of MCM-22P as 1.0 wt% can maximize the crystallization performance of PET, while much more content of MCM-22P may lead to the aggregation of MCM-22P and thus weakening the crystallization performance of PET.

Local structure of zeolites and O–H in nanocomposites

It is observed that MCM-22P has superior compatibility with PET matrix due to the array of abundant silanol on external surface, contributing to remarkable crystallization performance of PET/M22P nanocomposites [30,40]. The ^{29}Si one-pulse NMR spectra of Y, ZSM-5 and MCM-22P are displayed in a, b and c of Fig. 5. The peaks at −100 ~ -110 ppm and −110 ~ -120 ppm are assigned to Q_3 and Q_4 species respectively, in which Q_n means $Si(OSi)_n(OH)_{4-n}$. ^{29}Si NMR experiment on MCM-22P is of fundamental importance because ^{29}Si NMR spectra can provide complementary structural information such as the content of hydroxyl group. A ^{29}Si CP NMR study was presented in the zoom-in picture in Fig. 5c to investigate the content of hydroxyl group. The peaks of Q_3 and Q_4 species can be further curve-fitted into the peaks for Q_a, Q_b, Q_c, Q_d and Q_e respectively, as shown in Supporting Information Fig. S6, in which Q_b is attributed to hydroxyl group. Furthermore, the content of hydroxyl group in MCM-22P can be calculated by the ratio Q_b to Q_n equal to 16.7%, improving the compatibility with PET matrix. The ^{29}Si spectrum of zeolite Y contains five silicon environments among the range −85 ~ -105 ppm, determined by the amount of Al atoms in the second coordination sphere [41]. In addition, the two peaks among the range −105 ~ -115 ppm shown in ZSM-5 are attributed to its silicon environments in the framework as well [42].

The corresponding ^{27}Al one-pulse NMR spectra of the Y, ZSM-5 and MCM-22P are shown in Supporting Information Fig. S7, respectively. The ^{27}Al one-pulse NMR spectra of aluminosilicates framework usually comprise one tetrahedral (T_d) Al resonance between the 54 to 68 ppm which illustrates the surrounding environment of an aluminum atom in the tetrahedral framework [43]. There is the only one signal at 60 ppm in the ^{27}Al NMR spectrum of Y zeolite

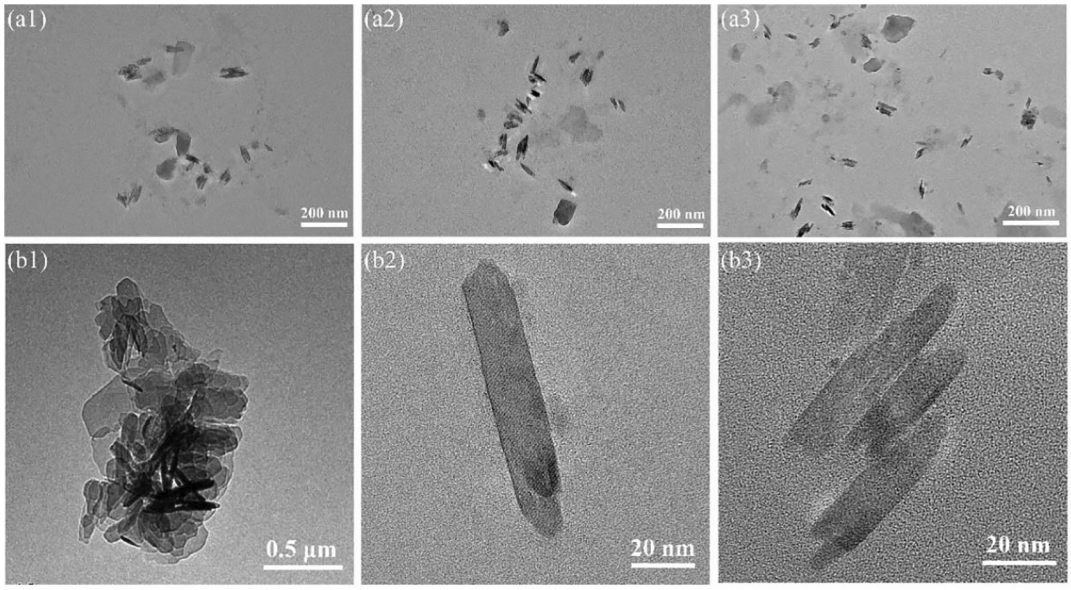

Fig. 4. TEM images for dispersal morphologies of zeolites in PET: (a1) PET/1%Y, (a2) PET/1%ZSM-5, (a3) PET/1%MCM-22P and (b1) morphology of MCM-22P, exfoliation morphologies of MCM-22P in (b2) PET/M22P1.0 and (b3) PET/M22P2.0.

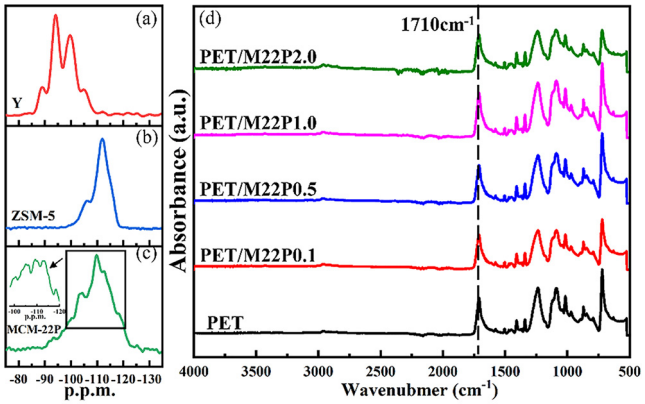

Fig. 5. ^{29}Si NMR spectra of (a) Y, (b) ZSM-5, (c) MCM-22P and (d) FTIR ATR spectra of PET/M22P nanocomposites with different content of MCM-22P.

and the peak reflects Al atom in tetrahedral coordination of the framework [44]. Besides, the sharp peak that appeared at 55 ppm in ZSM-5 is assigned to the Al in the zeolite framework. While the ^{27}Al NMR spectrum of MCM-22P is comprised of two T_d resonances centred at about 50 and 56 ppm. All these above spectral data are consistent with literature [42].

Infrared spectra can be used to investigate the hydrogen bonding which could form between the Si-O–H surface of MCM-22P and O atoms in PET molecular chain and lead to local ordered structure in PET/M22P nanocomposites possibly. The FTIR ATR results of neat PET and PET/M22P nanocomposites containing different content of MCM-22P are shown in Fig. 5d. The C–H stretching, C–H bending and C–C bending vibrations of benzene rings in PET appear at 3055 cm^{-1}, 792 cm^{-1}, 846 cm^{-1} and 721 cm^{-1}, respectively. The absorption peaks at 3429 cm^{-1} and 970 cm^{-1} represent O–H bonded to C = O groups and in terminal carboxylic groups in PET chain [45]. The peak at 1710 cm^{-1} was assigned to C = O symmetric stretching of carbonyl groups, which could be further curve-fitted into the bands for free and hydrogen-bonded components centred at about 1716 and 1706 cm^{-1} respectively. The hydrogen bond fraction F_{O-HO} is determined from Eq. (4):

$$F_{O-HO} = (A_H/r_{H/a})/(A_H/r_{H/a} + A_a) \quad (4)$$

where A_a and A_H represent the absorption peak of 1716 and 1706 cm^{-1} respectively, and $r_{H/a}$ is the specific absorption ratio of the two bands, which is 1.35 as reported [46]. The calculated results of hydrogen bond fraction are 0.33 for PET, 0.37 for PET/M22P0.1, 0.38 for PET/M22P0.5, 0.40 for PET/M22P1.0 and 0.41 for PET/M22P2.0. It is obvious that F_{O-HO} increased after the addition of MCM-22P, indicating the strong interfacial reaction between MCM-22P and PET matrix due to a number of interfacial hydrogen bonds. The interaction has a great significance on increasing the compatibility between PET and MCM-22P, resulting in better dispersion of MCM-22P in PET and faster crystallization rate of PET/M22P nanocomposites.

Effect of MCM-22P contents on non-isothermal crystallization of PET

In order to further explore the influence of the MCM-22P on the crystallization of PET, nanocomposites within different content of MCM-22P were investigated under non-isothermal conditions, which is associated with the dispersion of MCM-22P and the compatibility with PET matrix. The DSC curves for PET and PET/M22P1.0 at different cooling rates were shown in a-b of Fig. 6 and Table 4, and other nanocomposites were shown in Supporting Information Fig. S8. As cooling rate increased from 5 °C/min to 30 °C/min, the obtained T_{mc} of PET reduced from 184.6 °C to 172.5 °C, and T_{mc} of PET/M22P1.0 decreased from 219.0 °C to 186.7 °C as shown in Fig. 6c. In addition, X_C for PET reduced from 32.8% to 14.6%, while X_C for PET/M22P1.0 decreased from 41.4% to 31.7% at such cooling rates. The peak of melt-crystallization becomes obviously broader and transfers to lower temperatures because a higher degree of supercooling is requested to accomplish the crystallization process at a higher cooling rate. It is confirmed that the order of molecular and rate of crystallization process in PET/M22P1.0 is higher and faster compared to PET as well.

Mozhishen method termed as Eq. (5) [47], is used to analyze the complicated non-isothermal melt-crystallization process:

$$\ln\phi = \ln F(T) - \alpha \ln t \quad (5)$$

ϕ is cooling rate, t is crystallization time, $F(T)$ is the cooling rate required for a polymer system to reach a certain degree of crystallinity per unit time, which can characterize the difficulty of achieving a certain degree of crystallinity within a certain period. The plot of $\ln\phi$ versus $\ln t$ of PET/M22P1.0 was shown in Fig. 6d and all other PET/M22P nanocomposites by Mozhishen method were shown in Fig. S9 of Supporting Information. It is obvious that $F(T)$ of all samples increases with the increase of relative crystallinity from Table 5 and Table SIII in Supporting Information, because the faster cooling rate is required for higher relative crystallinity per time. In addition, the $F(T)$ of the PET at the same crystallinity is greater than that of the PET/M22P nanocomposites, indicating that the addition of the MCM-22P accelerates the crystallization rate of the PET. The value of $F(T)$ has an important relationship with $W_{1/2mc}$ during the cooling crystallization process. Smaller $F(T)$ corresponds to narrower peak, reflecting faster crystallization rate and shorter crystallization time.

Isothermal crystallization behavior of PET/M22P nanocomposites

The isothermal crystallization can characterize the crystallization process and nucleation mechanism of polymer mathematically, in which Avrami analysis is the most universal theory as explained in Supporting Information. The region of relative crystallinity $X(t)$ from 0.02 to 0.3 was selected for the investigation, because crystal nuclei are unstable in the initial period and impingement of growing centres can cause cessation of growth in the terminal period of crystallization process. Avrami exponent n and crystallization kinetic constant $\ln K_t$ can be obtained from graph $\ln\{-\ln[1 - X(t)]\}$ versus $\ln t$ according to Eq. (S1) as shown in Fig. 7. The half-time of crystallization $t_{1/2}$ is obtained from Eq. (S2), which can also estimate the crystallization rate.

In order to investigate the influence of isothermal crystallization temperature T_c on the crystallization manner, plots of $\ln\{-\ln[1 - X(t)]\}$ versus $\ln t$ at different T_c are shown in Fig. S10 and Table SIV of Supporting Information in which PET/M22P1.0 is shown in Fig. 7a. It is clear that K_t increases and $t_{1/2}$ decreases after the addition of MCM-22P from the relationship of K_t versus T_c and $t_{1/2}$ versus T_c as shown in b-c of Fig. 7. Besides, K_t becomes larger and $t_{1/2}$ becomes smaller at the same T_c as the content of MCM-22P increases when MCM-22P is less than 1.0 wt.%. However, compared to PET/M22P2.0,K_t of PET/M22P1.0 is larger and $t_{1/2}$ is smaller, reflecting better dispersion of 1.0 wt.% MCM-22P in PET matrix than 2.0 wt.% as the above results. In particular, when the addition of MCM-22P is 1.0 wt.%, $t_{1/2}$ has been shortened from 773 s of PET to 168 s of PET/M22P1.0 at 220 ℃ corresponding to different crystallization mechanisms in Fig. 7c. The crystallization of PET/M22P nanocomposites is proceeded via the mechanism of heterogeneous nucleation compared to homogeneous nucleation mechanism of neat PET, thus the amount of nucleation sites in PET/M22P is much more than PET.

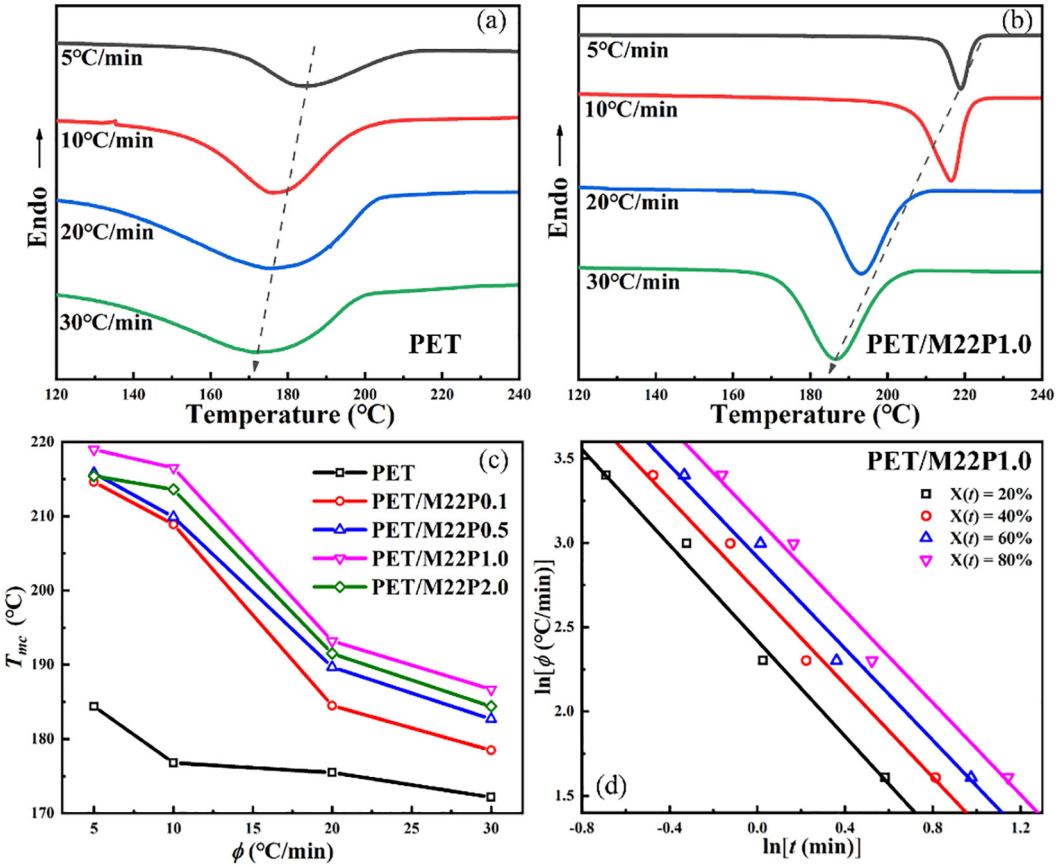

Fig. 6. Non-isothermal crystallization curves for (a) PET, (b) PET/M22P1.0, (c) melt-crystallization temperature T_{mc} versus cooling rate ϕ for PET and PET/M22P nanocomposites and (d) the plots of lnϕ versus ln$t$ by Mozhishen method for PET/M22P1.0.

Table 4
Non-isothermal crystallization parameters for PET and PET/M22P1.0 nanocomposite at different cooling rates.

Samples	Φ [a]℃/min	T_{onset}℃	T_{mc}℃	$W_{1/2mc}$ [b]℃	ΔH_{mc} J/g	X_C%
PET	5	212.6	184.6	27.0	38.6	32.8
	10	205.4	176.6	31.8	34.6	29.4
	20	204.0	175.5	40.3	20.4	17.3
	30	200.6	172.5	43.0	17.2	14.6
PET/M22P1.0	5	226.6	219.0	10.6	48.7	41.4
	10	225.2	216.5	15.3	47.6	40.5
	20	210.1	193.2	18.9	39.8	33.8
	30	206.4	186.7	22.3	37.3	31.7

[a]Cooling rate, [b] half-width of crystallization peak.

Table 5
Parameters of non-isothermal crystallization from Mozhishen method for neat PET and PET/M22P1.0.

$X(t)$%	$F(T)$℃/min	
	PET	PET/M22P1.0
20	3.25	2.42
40	3.55	2.71
60	3.88	2.92
80	4.11	3.14

The crystallization kinetics of PET, PET/M22P0.1 and PET/M22P1.0 were further explored by the theory of Hoffman-Lauritzen (H-L equation) as Supporting Information Eq. (S3). H-L equation can be transformed into the form of double-logarithmic as expressed in Eq. (6):

$$\ln G + \frac{U^*}{R(T_c - T_\infty)} = \ln G_0 - \frac{K_g}{T_c \Delta T f} \quad (6)$$

The equilibrium melt-temperature T_m^0 can be calculated by the linear relation between T_m and T_c depending on Hoffman-Weeks plots [48], and the intersection point at linear extrapolation of Hoffman-Weeks plot where $T_m = T_c$ is T_m^0 as shown in Supporting Information Fig. S11. The T_m^0 for neat PET is 548.2 K, approaching the value of 547.2 K [49], and the calculated values of T_m^0 for PET/M22P nanocomposites are approximately 541 K due to different selected isothermal crystallization temperature ranges [4,50]. Fig. 7d shows the linear relation corresponding to the $\ln G + U^*/R(T_c - T_\infty)$ vs $1/(T_c \Delta T f)$ and the equation of constant nucleation rate K_g as the slope of the lines is expressed in Eq. (S4). The fold surface free energy σ_e of neat PET was determined to be 110.0 J/m^{-2} in our previous work [9] while PET/M22P0.1

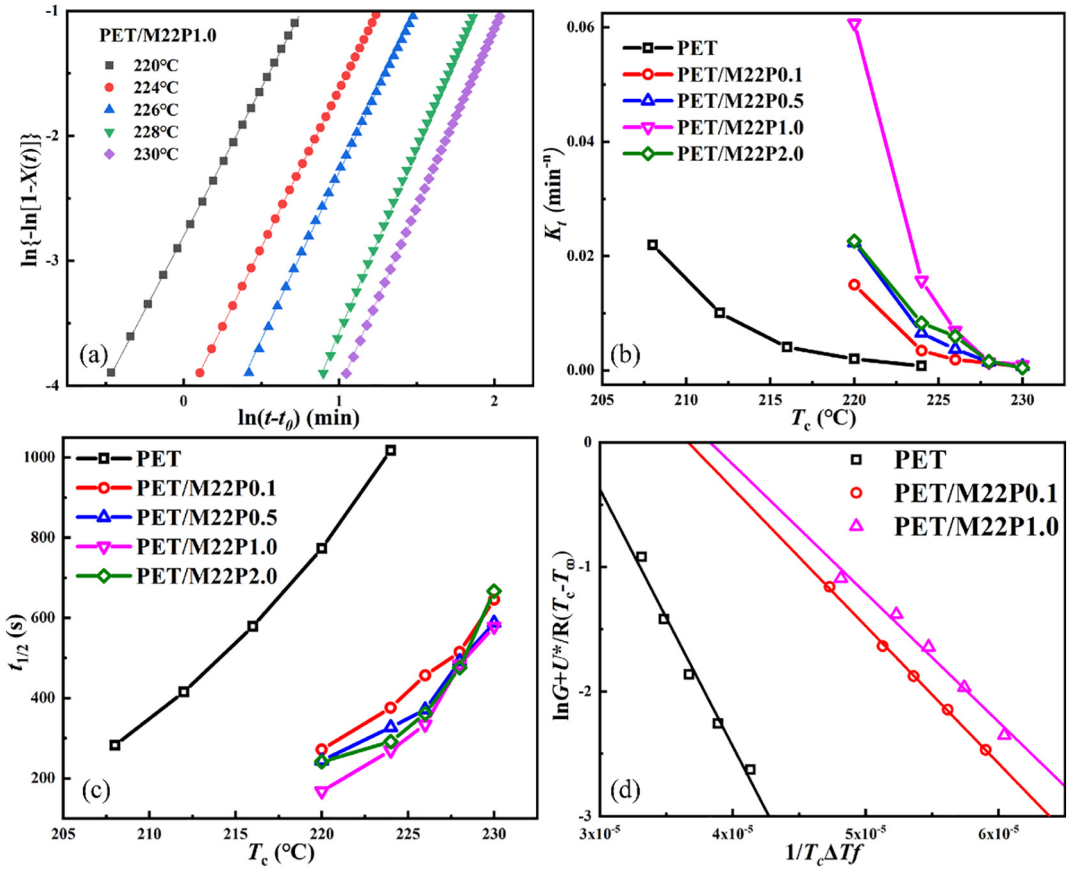

Fig. 7. (a) Avrami plots of $\ln\{-\ln[1-X(t)]\}$ versus ln$t$ in isothermal crystallization for PET/M22P1.0, (b) crystallization kinetic constant K_t versus isothermal crystallization temperature T_c and (c) half-time of crystallization $t_{1/2}$ versus T_c for PET/M22P nanocomposites, (d) L–H plots of $\ln G + U^*/R(T_c - T_\infty)$ versus $1/T_c\Delta Tf$ of PET, PET/M22P0.1, PET/M22P1.0.

and PET/M22P1.0 decreased to 22.1 J/m^{-2} and 20.7 J/m^{-2}, respectively. The addition of MCM-22P can decrease σ_e as an effective nucleation agent by providing more nucleation nuclei for PET as shown in Table 6 and improve the crystallization rate of PET [51,52]. Moreover, σ_e decreases gradually when the incorporation of MCM-22P increases, reflecting the outstanding compatibility between 2D zeolite MCM-22P and PET.

These results reflect that the influence of nucleation and crystallization is advanced with the incorporation of MCM-22P, because 2D zeolite MCM-22P is of layer topology and the exfoliation in melt processing can further provide much more platelets, resulting in more nucleation sites for PET. It is demonstrated that the crystallization process of PET is much more sensitive to crystallization temperature T_c than PET/M22P nanocomposites because PET requests a larger degree of supercooling to complete the orientation motion of polymer chain than PET/M22P nanocomposites, as analyzed in the non-isothermal section above.

Table 6
Equilibrium melting temperature T_m^0, kinetic parameter K_g and fold surface free energy σ_e of PET, PET/M22P0.1 and PET/M22P1.0.

	PET	PET/M22P0.1	PET/M22P1.0
T_m^0 (K)	548	540	540
K_g (10^5)	2.06	1.10	1.03
σ_e (J/m^{-2})	80.9	22.1	20.7

Conclusion

In present work, a variety of zeolites with different topologies were considered as effective nucleation agents for PET crystallization. The addition of 3D zeolites Y, ZSM-5, and 2D zeolite MCM-22P results in a considerable improvement on the crystallization performance, thermal stability and oxygen barrier properties of PET, which is attributed to specific surface area of zeolites and superior dispersion of zeolites in PET. Among them, 2D zeolite MCM-22P exhibits best nucleation performance due to its layered morphology and excellent compatibility with PET by surface groups of MCM-22P. In addition, MCM-22P can be further exfoliated during the melt compounding, providing more nucleation sites for PET. By means of Mozhishen method, Avrami equation and theory of Hoffman–Lauritzen, the calculated nucleation and surface free energy of the PET chains were decreased obviously after the incorporation of MCM-22P, thus decreasing the energy barrier in the nucleation process. Therefore, PET/zeolite nanocomposites have great industrialization potentials in packaging films and engineering plastics. The work is worthy of further investigation to be applied in similar polymer/zeolite nanocomposites, providing guidance for the research of porous materials as nucleating agents.

Declaration of Competing Interest

The authors declare that they have no known competing financial interests or personal relationships that could have appeared to influence the work reported in this paper.

Acknowledgments

The authors thank the financial support from the National Natural Science Foundation of China (Grant nos. 21774027, 21973017, 22175040 and 21802023).

Appendix A. Supplementary data

Supplementary data to this article can be found online at https://doi.org/10.1016/j.jiec.2022.02.038.

References

[1] A. Hadjizadeh, A. Ajji, M.N. Bureau, J. Mech. Behav. Biomed. Mater., 3 (2010) 574-583 10.1016/j.jmbbm.2010.07.002.
[2] Y. Wang, J. Shen, J. Yuan, J. Colloid Interface Sci. 480 (2016) 205–217, https://doi.org/10.1016/j.jcis.2016.07.022.
[3] M. Wang, W. Hu, Y. Ma, Y.-Q. Ma, Macromolecules 38 (2005) 2806–2812, https://doi.org/10.1021/ma047444q.
[4] V.D. Deshpande, S. Jape, J. Appl. Polym. Sci. 116 (2010) 3541–3554, https://doi.org/10.1002/app.31891.
[5] D. Garcia, J. Polym. Sci. Pol. Phys. 22 (1984) 2063–2072, https://doi.org/10.1002/pol.1984.180221206.
[6] N.K. Kalfoglou, D.S. Skafidas, Eur. Polym. J. 30 (1994) 933–939, https://doi.org/10.1016/0014-3057(94)90027-2.
[7] Y. Yu, H.S. Bu, Macromol. Chem. Phys., 202 (2001) 421-425 10.1002/1521-3935(20010201)202:3421::Aid-macp4213.0.Co;2-v.
[8] S. Xing, R. Li, P. Tang, Macromol. Chem. Phys. 216 (2015) 301–313, https://doi.org/10.1002/macp.201400444.
[9] W. Zhang, H. Zhang, Y. Yang, P. Tang, Polymer Bull. (2021), https://doi.org/10.1007/s00289-021-03672-3.
[10] S.L. Xing, R. Li, J.J. Si, P. Tang, Journal of Industrial and Engineering Chemistry, 38 (2016) 167-174 10.1016/j.jiec.2016.04.020.
[11] H. Ghasemi, P.J. Carreau, M.R. Kamal, S.H. Tabatabaei, Polym. Eng. Sci. 52 (2012) 420–430, https://doi.org/10.1002/pen.22099.
[12] R.R. Chowreddy, K. Nord-Varhaug, F. Rapp, J. Mater. Sci. 53 (2018) 7017–7029, https://doi.org/10.1007/s10853-018-2014-0.
[13] Z. Tong, W. Zhuo, J. Zhou, R. Huang, G. Jiang, J. Mater. Sci. 52 (2017) 10567–10580, https://doi.org/10.1007/s10853-017-1173-8.
[14] Y.H. Shin, W.D. Lee, S.S. Im, Macromol. Res. 15 (2007) 662–670, https://doi.org/10.1007/bf03218947.
[15] J. Jiang, G. Li, H. Liu, Q. Ding, K.C. Mai, Compos. Pt. A-Appl. Sci. Manuf. 45 (2013) 88–94, https://doi.org/10.1016/j.compositesa.2012.10.002.
[16] Z. Lv, L. Zhang, Y. Yang, X. Bi, Mater. Des. 32 (2011) 3624–3628, https://doi.org/10.1016/j.matdes.2011.02.016.
[17] Z. Lv, K. Wang, Z. Qiao, W. Wang, Mater. Des. 31 (2010) 3804–3809, https://doi.org/10.1016/j.matdes.2010.03.028.
[18] M.G. Mohamed, E.C. Atayde, B.M. Matsagar, J. Na, Y. Yamauchi, K.C.W. Wu, S. W. Kuo, Journal of the Taiwan Institute of Chemical Engineers, 112 (2020) 180-192 10.1016/j.jtice.2020.06.013.
[19] B. Han, C. Yin, J. Chang, Y. Pang, P. Lv, W. Song, X. Wang, Polymers 12 (2020) 2108, https://doi.org/10.3390/polym12092108.
[20] T. Hao, Y. Wang, Z. Liu, J. Li, L. Shan, W. Wang, J. Liu, J. Tang, Nanomaterials 11 (2021) 2810, https://doi.org/10.3390/nano11112810.
[21] M.G. Mohamed, S.W. Kuo, Macromol. Chem. Phys. 220 (2019) 1800306, https://doi.org/10.1002/macp.201800306.
[22] A. Chaurasia, R.S. Mulik, A. Parashar, Mechanics of Advanced Materials and Structures, (2021) 1-26 10.1080/15376494.2021.1871688.
[23] M. Vinyas, S.J. Athul, D. Harursampath, M. Loja, T. Nguyen Thoi, Mater. Res. Express, 6 (2019) 092002 10.1088/2053-1591/ab3175.
[24] G.Z. Papageorgiou, E. Karandrea, D. Giliopoulos, D.G. Papageorgiou, A. Ladavos, A. Katerinopoulou, D.S. Achilias, K.S. Triantafyllidis, D.N. Bikiaris, Thermochim. Acta, 576 (2014) 84-96 10.1016/j.tca.2013.12.006.
[25] C.I.W. Calcagno, C.M. Mariani, S.R. Teixeira, R.S. Mauler, Polymer 48 (2007) 966–974, https://doi.org/10.1016/j.polymer.2006.12.044.
[26] X. Zhang, S. Zhao, M.G. Mohamed, S.-W. Kuo, Z. Xin, J. Mater. Sci. 55 (2020) 14642–14655, https://doi.org/10.1007/s10853-020-05003-9.
[27] G.T. Kokotailo, S.L. Lawton, D.H. Olson, W.M. Meier, Nature 272 (1978) 437–438, https://doi.org/10.1038/272437a0.
[28] E.M. Flanigen, B.M. Lok, R.L. Patton, S.T. Wilson, Pure Appl. Chem. 58 (1986) 1351–1358, https://doi.org/10.1351/pac198658101351.
[29] J.W. Ward, J. Catal., 9 (1967) 225-& 10.1016/0021-9517(67)90248-5.
[30] A. Corma, V. Fornes, S.B. Pergher, T.L.M. Maesen, J.G. Buglass, Nature 396 (1998) 353–356, https://doi.org/10.1038/24592.
[31] A. Corma, C. Corell, J. Pérez-Pariente, Zeolites 15 (1995) 2–8, https://doi.org/10.1016/0144-2449(94)00013-i.
[32] S. Maheshwari, E. Jordan, S. Kumar, F.S. Bates, R.L. Penn, D.F. Shantz, M. Tsapatsis, J. Am. Chem. Soc. 130 (2008) 1507–1516, https://doi.org/10.1021/ja077711i.
[33] N.-L. Michels, S. Mitchell, M. Milina, K. Kunze, F. Krumeich, F. Marone, M. Erdmann, N. Marti, J. Pérez-Ramírez, Advanced Functional Materials, 22 (2012) 2509-2518 10.1002/adfm.201103120.
[34] Z. Bartczak, A. Galeski, N.P. Krasnikova, Polymer 28 (1987) 1627–1634, https://doi.org/10.1016/0032-3861(87)90002-4.
[35] E. Martuscelli, C. Silvestre, L. Bianchi, Polymer 24 (1983) 1458–1468, https://doi.org/10.1016/0032-3861(83)90231-8.
[36] A. Taniguchi, M. Cakmak, Polymer 45 (2004) 6647–6654, https://doi.org/10.1016/j.polymer.2004.06.056.
[37] C. Kang, J. Xu, L. Niu, C. Li, J. Fan, Polym. Compos. (2021), https://doi.org/10.1002/pc.26042.
[38] Y.C. Ke, C.F. Long, Z.N. Qi, J. Appl. Polym. Sci., 71 (1999) 1139-1146 10.1002/(sici)1097-4628(19990214)71:71139::Aid-app123.0.Co;2-e.
[39] J.Y. Kim, H.S. Park, S.H. Kim, Polymer 47 (2006) 1379–1389, https://doi.org/10.1016/j.polymer.2005.12.042.
[40] V.J. Margarit, M.E. Martínez-Armero, M.T. Navarro, C. Martínez, A. Corma, Angew. Chem. Int. Ed. 54 (2015) 13724–13728, https://doi.org/10.1002/anie.201506822.
[41] K. Gaare, D. Akporiaye, J. Phys. Chem. B 101 (1997) 48–54, https://doi.org/10.1021/jp962028w.
[42] S.L. Burkett, M.E. Davis, Chem. Mat. 7 (1995) 920–928, https://doi.org/10.1021/cm00053a017.
[43] G.J. Kennedy, S.L. Lawton, A.S. Fung, M.K. Rubin, S. Steuernagel, Abstracts of Papers of the American Chemical Society, 215 (1998) U482-U482.
[44] Z. Konya, I. Hannus, I. Kiricsi, P. Lentz, J.B. Nagy, Colloids and Surfaces a-Physicochemical and Engineering Aspects, 158 (1999) 35-42 10.1016/s0927-7757(99)00128-4.
[45] M. Parvinzadeh, S. Moradian, A. Rashidi, M.-E. Yazdanshenas, Appl. Surf. Sci. 256 (2010) 2792–2802, https://doi.org/10.1016/j.apsusc.2009.11.030.
[46] H.-Y. Yu, H. Zhang, M.-L. Song, Y. Zhou, J. Yao, Q.-Q. Ni, ACS Appl. Mater. Interfaces 9 (2017) 43920–43938, https://doi.org/10.1021/acsami.7b09102.
[47] Z. Zhang, L. Feng, Y. Li, Y. Wang, C. Yan, Polym. Compos. 36 (2015) 510–516, https://doi.org/10.1002/pc.22966.
[48] J.D. Hoffman, J.J. Weeks, J. Res. Nat. Bur. Stand. Sec. 66A (1962) 13–28, https://doi.org/10.6028/jres.066A.003.
[49] V.E. Reinsch, L. Rebenfeld, J. Appl. Polym. Sci. 52 (1994) 649–662, https://doi.org/10.1002/app.1994.070520508.
[50] X.L. Jiang, S.J. Luo, K. Sun, X.D. Chen, Express Polym. Lett. 1 (2007) 245–251, https://doi.org/10.3144/expresspolymlett.2007.37.
[51] B. Yu, X. Wang, X. Qian, W. Xing, H. Yang, L. Ma, Y. Lin, S. Jiang, L. Song, Y. Hu, S. Lo, RSC Adv. 4 (2014), https://doi.org/10.1039/c3ra45945d.
[52] L. Cao, D. Su, Z. Su, X. Chen, Ind. Eng. Chem. Res. 53 (2014) 2308–2317, https://doi.org/10.1021/ie403746p.